Journal of Materials Chemistry C

ROYAL SOCIETY OF CHEMISTRY

PAPER

Cite this: J. Mater. Chem. C, 2020, 8, 9602

Chirality control in white-light emitting 2D perovskites†

Karla Trujillo-Hernández,‡[a] Germán Rodríguez-López,‡[a] Arian Espinosa-Roa,[a] Jesús González-Roque,[a] A. Paulina Gómora-Figueroa,[b] Weiguo Zhang,[c] P. Shiv Halasyamani,[c] Vojtech Jancik,[de] Milan Gembicky,[f] Giuseppe Pirruccio[g] and Diego Solis-Ibarra*[a]

Received 30th April 2020, Accepted 4th June 2020

DOI: 10.1039/d0tc02118k

rsc.li/materials-c

The increased interest in white solid-state lighting devices addresses the urgent challenge to develop semiconductors with broad band emission. In recent years, low dimensional hybrid organic/inorganic lead perovskites have shown great potential as single white-light emitters. Herein, we show that it is possible to control the chirality of lead bromide perovskites by incorporating enantiopure (*R* or *S*) or racemic (*RS*) β-methylphenethylammonium. The incorporation of such cations allows us to control the chirality of the resulting materials and yields the first examples of 2D chiral perovskites that emit white light. Furthermore, we demonstrate that these materials exhibit second harmonic generation. Our results demonstrate the potential of this kind of materials for chiroptical applications and non-linear optics.

Introduction

Halide perovskites have rapidly emerged as promising absorbers for solar cells[1–3] and phosphors for lighting applications.[4–6] In recent years, halide perovskites have been used as down converters in mixed-phosphor devices due to their high colour purity (narrow emission) and emission tunability.[4–6] Nevertheless, the conventional mixed-phosphor approach for white-light emitting diodes (WLEDs) has significant limitations such as varying light quality over time and efficiency losses. The former is due to the differential aging of mixed phosphors and the latter is due to cross- and self-absorption.[6,7] Since the first report of a hybrid organic/inorganic lead perovskite (HOIP) exhibiting intrinsic white light emission,[8] 2D and 1D perovskites have become promising single white-light emitting materials, which could overcome the drawbacks of WLEDs.[4–6,9,10] Particularly the broad band emission of 2D perovskites is observed due to the deformable nature of the inorganic lattice that allows strong exciton phonon coupling, which can ease the formation of self-trapped states and multiple colour centres.[11] Furthermore, structural deformation in the Pb-Br length and the Pb-[μ-Br]-Pb angles of the inorganic octahedral structures "[$PbBr_6$]" has been associated with the broad band emission from these materials.[9,12–14] Although the broad band emission comes from the inorganic layer, the steric effect of the organic cation induces distortion on the inorganic layers, subsequently fostering the broad band emission.[15]

Furthermore, the organic cation of the HOIPs determines some properties like the dimensionality or the orientation of the inorganic layer framework (⟨110⟩, ⟨100⟩), which directly affects the electronic structures and, hence, the emissive properties of 2D perovskites.[14,16–18] Therefore, we hypothesize that a chiral cation could be a powerful tool to induce chirality and strain in the inorganic layer. On one hand, the strain would promote white light emission and, on the other hand, the chirality of the organic molecule would generate non-centrosymmetric structures, capable of presenting chiroptical response.[19–21] The insertion of an enantiopure molecule into a perovskite avoids inversion in the material, forcing the perovskite to crystallize in a Sohncke space group, whereas the insertion of a racemic mixture (presence of a pair of enantiomers) allows inversion and crystallization in centrosymmetric structures, thus obtaining achiral materials.[22]

[a] Instituto de Investigaciones en Materiales, Universidad Autónoma de México, (UNAM), Coyoacán, 04510, Ciudad de México, Mexico. E-mail: diego.solis@unam.mx
[b] Facultad de Ingeniería, Universidad Nacional Autónoma de México (UNAM), Coyoacán, 04510, Ciudad de México, Mexico
[c] Department of Chemistry, University of Houston, Houston, Texas 77204, USA
[d] Universidad Nacional Autónoma de México, Instituto de Química, Ciudad Universitaria, Ciudad de México, 04510, Mexico
[e] Centro Conjunto de Investigación en Química Sustentable UAEM-UNAM, Carretera Toluca-Atlacomulco km. 14.5, Toluca, Estado de México, Mexico
[f] Department of Chemistry and Biochemistry, University of California, 9500 Gilman Drive, Mail Code 0358, La Jolla, San Diego, CA, 92093, USA
[g] Instituto de Física, Universidad Autónoma de México (UNAM), Coyoacán, 04510, Ciudad de México, Mexico

† Electronic supplementary information (ESI) available. CCDC 1995234, 1995235 and 1995236. For ESI and crystallographic data in CIF or other electronic format see DOI: 10.1039/d0tc02118k

‡ These authors contributed equally to this work.

Chiral ammonium cations have been successfully incorporated into lead halide nanowires and lead iodide perovskites to obtain materials with properties such as second harmonic generation (SHG),[23] circularly polarized photoluminiscense[24] and bulk photovoltaic effects.[25] Surprisingly, as far as we know, only one chiral perovskite with white-light emission has been reported, and in that case only one isomer was synthesized.[26] Despite these early developments, the exploration of the effect of chiral cations in hybrid perovskites is still a promising field due to the vast chemical diversity and superb optoelectronic properties of this type of perovskites.[19,20]

In this work, we synthesized three lead bromide perovskites that incorporate the *R*-(+) and *S*-(−) enantiomers or a racemic mixture (*R*-(+),*S*-(−)) of β-methylphenethylammonium (β-MPEA) to form $[(R)\text{-β-MPEA}]_2PbBr_4$ (**1R**), $[(S)\text{-β-MPEA}]_2PbBr_4$ (**1S**), and $[(R,S)\text{-β-}[MPEA]_2PbBr_4]$ (**1RS**), respectively. All three perovskites were thoroughly characterized, and it was demonstrated that the chiral cations could transfer their non-centrosymmetric nature to the material and, at the same time, produce white light photoluminescence.

Experimental section

Materials

The following reagents were purchased from commercial vendors and used without any further purification: lead bromide (≥98%), hydrobromic acid (ACS 48%), β-methylphenethylamine (99%), (*R*)-(+)-β-methylphenethylamine (99%) and *S*-(−)-β-methylphenethylamine (99%). The solvents used were ethyl acetate (EtOAc), *N*,*N*-dimethylformamide (DMF), petroleum ether and acetonitrile (CH_3CN). All manipulations were conducted in air.

Instruments

The infrared spectroscopy experiments were performed using a Bruker Alpha spectrometer with an attenuated total reflection (ATR) module and a diamond window in the range of $\tilde{\nu}$ 4000–400 cm^{-1}, measuring 32 sweeps per sample with a resolution of 2 cm^{-1}. For powder X-ray diffraction (PXRD) a Bruker D8 Advance (with the Diffrac Plus Release 2000 software) and a Rigaku ULTIMA IV diffractometer with CuKα radiation (λ = 1.54183 Å) were used at room temperature. The data were collected in the 3° to 45° range at a rate of 1° min^{-1}. The thermogravimetric measurement (TGA) was carried out using a Q5000 TGA from TA Instruments with a N_2 flow rate of 25 mL min^{-1} and a heating rate of 3° min^{-1} from 25 to 600 °C.

To measure the thin film absorbance spectra, a Shimadzu UV-2600 with an integrating sphere and a system of two halogen and deuterium lamps covering a wavelength range of 200–1400 nm was used. The photoluminescence measurement was performed using a 315 nm source and 10 mW power coupled to a photodetector. The photoluminescence quantum efficiency was measured using an FS5 spectrofluorometer with a 150 W CW ozone-free xenon arc lamp, Czerny–Turner design monochromators with flat grids for precise focusing at all wavelengths and minimum scattered light, with window spectral excitation in the range of 230–1000 nm and emission in the range of 230–870 nm, an R928P photomultiplier and an integration sphere. The measurements of circular dichroism were made using a BioLogic MOS-500 circular dichroism spectrophotometer with a xenon lamp with a wattage of 145.7 W and the temperature was controlled at 25 °C using a BioLogic TCU250 system. The second harmonic generation intensity experiments required a system composed of a Nd-YAG laser (1064 nm output), a photomultiplier, power supplies, optics and an oscilloscope placed on a flat surface.[27] The samples were placed in a fused silica tube.

Synthesis

$[(R,S)\text{-β-MPEA}]_2PbBr_4$ (**1RS**) was synthesized at 0 °C (ice bath) by reacting the mixture of $PbBr_2$ (100 mg, 0.272 mmol) and β-methylphenethylamine (80 μL, 0.544 mmol) in the ratio of 1 : 2 with 200 μL of HBr (48 wt% in water, Sigma-Aldrich) and 3 mL of CH_3CN in a 10 mL vial, and the solution was allowed to evaporate slowly overnight. The obtained microcrystals were washed with AcOEt, filtered and dried under vacuum, thus yielding a colourless crystalline powder. The same amounts were used and the same procedure was followed for the preparation of the (*R*)-(+)-β-methylphenethylamine (**1R**) and (*S*)-(−)-β-methylphenethylamine (**1S**) perovskites. The obtained crystalline solid was recrystallized by preparing a solution in CH_3CN and HBr. After two days, colourless crystals were obtained. Meanwhile, the deposition of thin films was performed with a Laurell WS-650 HZ-23NPP/UD2 spin coater. The required dimensions of the quartz substrates were 2.5 cm × 1.5 cm for the measurement of absorbance, whereas, for the circular dichroism experiments, quartz substrates with the dimensions of 1 cm × 2.5 cm were needed. The cleaning of the substrates consisted of washing them with different solvents (distilled water and ethanol) for 15 min in an ultrasonic bath and later subjecting them to UV plasma treatment for 15 min. Then 100 μL of 1 M (absorbance) and 0.5 M (circular dichroism) solutions were prepared separately from the respective perovskites **1RS**, **1R**, and **1S** in DMF; after that, 50 μL (1 M) or 30 μL (0.5 M) of the solutions were deposited by spin coating at a speed of 3500 rpm for 30 seconds on the quartz substrates. At the end of the deposition, the films were subjected to a heat treatment at 90 °C for 30 min.

$[(R,S)\text{-β-}C_6H_5(CH_3)CH_2CH_2NH_3]_2PbBr_4$ (1RS)

Colourless crystals. Yield: 0.1936 g (89%). Mp: 206 °C. FT-IR (ATR) $\tilde{\nu}$/cm^{-1}: 3174 (w, Ar–H), 3070 (m, Ar–H), 3027 (s, Ar–H), 2965 (m, CH_3), 2907 (m, CH_2), 2466 (w), 2343 (w), 1883 (w, Ar–C), 1807 (w), 1574 (m), 1472 (s), 1454 (s), 1394 (m), 1307 (m), 1278 (m), 1216 (w), 1138 (w), 1083 (w), 993 (m), 968 (m), 912 (w), 870 (w), 842 (w), 747 (s), 696 (vs), 533 (m), 456 (w).

$[(R)\text{-(+)-β-}C_6H_5(CH_3)CH_2CH_2NH_3]_2PbBr_4$ (1R)

Colourless crystals. Yield: 0.1885 g (87%). Mp: 204 °C. FT-IR (ATR) $\tilde{\nu}$/cm^{-1}: 3179 (w, Ar–H), 3072 (m, Ar–H), 3025 (s, Ar–H), 2986 (m, CH_3), 2916 (m, CH_2), 2467 (w), 2328 (w), 1952 (w, Ar–C), 1573 (m),

1481 (s), 1446 (s), 1391 (m), 1305 (m), 1215 (w), 1140 (m), 1086 (w), 1051 (w), 993 (m), 969 (m), 911 (w), 849 (w), 777 (w), 744 (vs), 699 (vs), 601 (m), 510 (m), 469 (w).

[(*R*)-(−)-β-$C_6H_5(CH_3)CH_2CH_2NH_3]_2PbBr_4$ (1S)

Colourless crystals. Yield: 0.1817 g (83%). Mp: 206 °C. FT-IR (ATR) $\tilde{\nu}$/cm^{-1}: 3171 (w, Ar–H), 3070 (m, Ar–H), 3027 (s, Ar–H), 2970 (m, CH_3), 2914 (m, CH_2), 2466 (w), 2333 (w), 1953 (w, Ar–C), 1804 (w), 1574 (m), 1471 (s), 1447 (s), 1392 (m), 1308 (m), 1139 (m), 1088 (w), 1053 (w), 994 (m), 970 (m), 914 (w), 846 (w), 745 (s), 696 (vs), 601 (m), 512 (m), 458 (w).

X-ray crystallography

A single crystal of **1R** was mounted on a Bruker APEX DUO diffractometer equipped with an Apex II CCD detector at 100 K. Frames were collected using CuKα radiation (Incoatec IμS with mirror optics) and omega scans (APEX 3).[28] A single crystal of **1S** was mounted on a Bruker X8 APEX diffractometer equipped with an Apex II CCD detector at 100 K. Frames were collected using MoKα radiation (a sealed tube with a graphite monochromator) using omega and phi scans (APEX 3).[28] In both cases, the data were integrated with SAINT.[28] Multi-scan absorption correction (SADABS)[28] was applied. A single crystal of **1RS** was mounted on an Agilent (currently RIGAKU) SuperNova Dual diffractometer equipped with an EosS2 CCD detector at 100 K. Frames were collected using MoKα radiation (SuperNova X-ray source) omega scans and integrated with CrysAlisPro (version 1.171.37.35).[29] The numerical absorption correction (SCALE3 ABSPACK)[30] was applied. The structures were solved by direct methods (SHELXT)[31] and refined using full-matrix least-squares on F^2 with SHELXL[32] using the ShelXle GUI[33] or OLEX2.[34] Weighted R factors, and all goodness-of-fit indicators, are based on F^2. All non-hydrogen atoms were refined anisotropically. The hydrogen atoms of the C–H and N–H bonds were placed in idealized positions and refined with U_{iso} tied to the parent atom. The disordered ammonium cations in **1RS** were refined using geometry (SAME, FLAT) and U_{ij} restraints (SIMU, RIGU, EADP) implemented in SHELXL.[32] Crystallographic information files (*.cif) for **1R**, **1S**, and **1RS** can be found under deposition numbers CCDC 1995234–1995236 or at DOI: 10.1039/d0tc02118k.†

Results and discussion

Characterization

The incorporation of the organic cation into the perovskite was first confirmed *via* IR-spectroscopy. Not surprisingly, all three IR spectra are almost identical (Fig. S1, ESI†), showing the expected characteristic bands for the organic cations. The most notable are the N–H and C_{aryl}–H bond vibrations (Fig. S1, ESI†) and the characteristic R–NH_3^+ bands, which partially overlap with the $\tilde{\nu}$(C–H_{aryl}) stretching that appears at $\tilde{\nu}$ 3024 cm^{-1}.

The three white solid materials (**1R**, **1S** and **1RS**) were analysed by powder X-ray diffraction. All the materials exhibit very similar diffraction patterns (Fig. 1) showing the characteristic

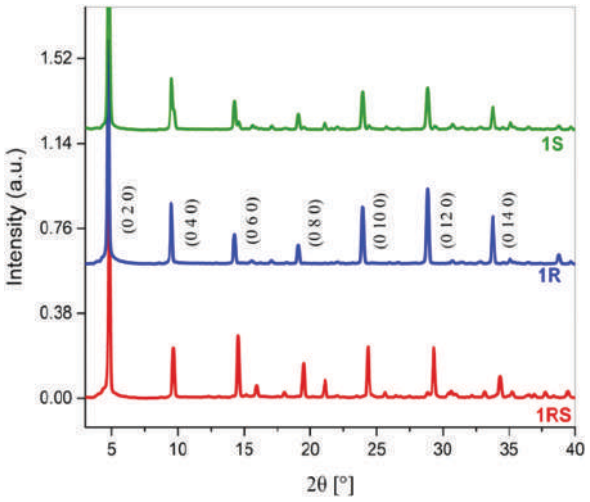

Fig. 1 Powder X-ray diffraction of **1S**, **1R**, and **1RS**.

preferential orientation of 2D perovskites. To gain a better insight into the structures of the perovskites, we crystallized the materials by a slow evaporation of concentrated solutions of each material in CH_3CN and HBr, resulting in the formation of colourless crystals, which were suitable for single crystal X-ray diffraction studies.

Crystal structures

All three structures crystallize in an orthorhombic lattice. As expected, the space group of the racemic mixture (**1RS**) is centrosymmetric (*Pbca*), while non-centrosymmetric space groups are obtained for the materials from the enantiopure ammoniums: **1R** ($P2_12_12$) and **1S** ($P2_12_12$), as shown in Fig. 2. The asymmetric units of **1R** and **1S** contain one chiral ammonium molecule and one $[PbBr_3]^{1-}$ anion, whereas **1RS** contains four ammonium cations and two $[PbBr_4]^{2-}$ anions in the asymmetric unit. The crystal structures of these materials also confirm that all of them have the expected 2D hybrid perovskite structure, with ⟨100⟩ oriented inorganic layers composed of corner-sharing $[PbBr_6]$ octahedra and the organic cation bilayer alternating with the inorganic layers (Fig. 2).

The crystal structure of **1RS** in Fig. 2C shows an important distortion of the inorganic sheets, which is accompanied by the alternation of two different ammonium conformations and shorter N–H···Br hydrogen bonds (see the X-ray diffraction data in the ESI†), while **1R** and **1S** exhibit only one organic cation conformation, with less distortion in the inorganic octahedra (Fig. 2). The distortion of the Pb–Br bond lengths was calculated using the equation:

$$\Delta d = \frac{1}{n}\sum\left[\frac{(d_n - d)}{d}\right]^2 \quad (1)$$

where d is the mean Pb–Br bond distance and d_n represents the six individual Pb–Br octahedral bond distances.[12] The Pb–Br bonds of the **1RS** structure are more distorted than those observed for **1R** and **1S**, which are relatively undistorted compared with the previously reported results[12,13] (see Table 1).

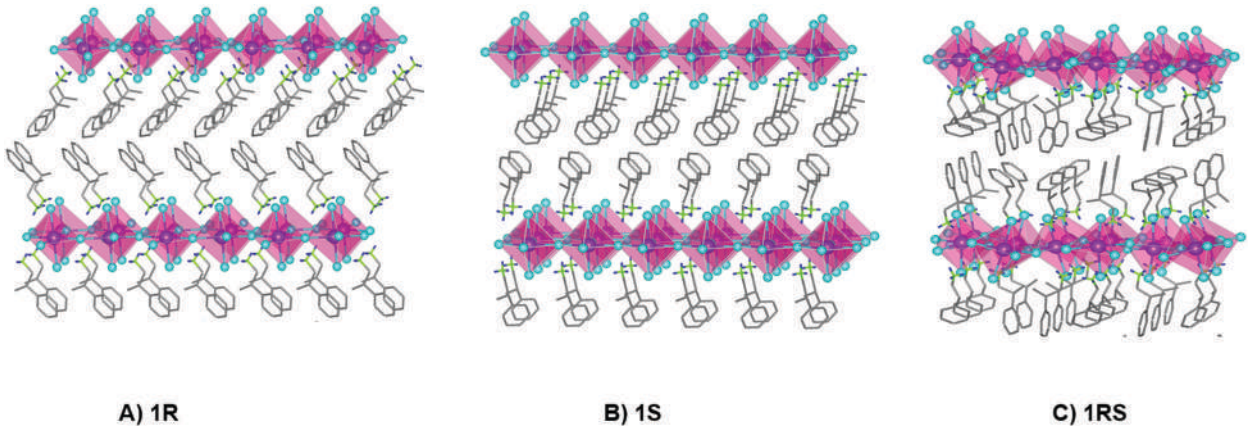

Fig. 2 Crystal structures of (A) **1R**, (B) **1S** and (C) **1RS**. Pink, aqua, green, grey and blue represent lead, bromine, nitrogen, carbon, and hydrogen, respectively. Carbon-bound hydrogen atoms were omitted for the sake of clarity.

However, the **1RS** distortion is similar to that observed for [NMEDA]$PbBr_4$ (a perovskite with broad band emission NMEDA = 1*N*-methylethane-1,2-diammonium).[35] The octahedral distortion of the inorganic [$PbBr_6$] sheets suggested that these materials could be white light emitters, which prompted us to study their optical properties.[12]

Absorption and SHG

The optical absorption of all three 2D HOIPs shows a characteristic semiconductor behaviour with the corresponding excitonic absorption at 390 nm (Fig. 3A).[36,37] Not surprisingly, all three materials, **1R**, **1S** and **1RS**, behave almost identically when looking at the absorption spectra. The chirality transfer of the organic cation to the whole perovskite was confirmed *via* circular dichroism (CD) and SHG. The chiral perovskites (**1R** and **1S**) exhibit a strong CD response in both excitonic and bandgap regions of the spectrum (Fig. 3B). As expected, the CD spectra of **1S** and **1R** are observed at nearly the same positions, although with oppositely signed values. The CD spectra of both **1R** and **1S** present a change to opposite signs, close to the exciton absorption, at 399 and 397 nm, respectively. This characteristic is known as "Cotton effect," and it is associated with a splitting of the fundamental transition of two bands that are preferentially excited by opposite circular polarization (Fig. 3B).[38]

We also evaluated the SHG properties of these materials. It is worth noting that SHG is a second order non-linear optical effect, and therefore it is necessary to have a non-centrosymmetric medium.[39] Surprisingly, all three perovskites (**1R**, **1S** and **1RS**) showed second harmonic generation, with 0.9, 0.7, and 1.1 times the efficiency of α-SiO_2, respectively. Since the **1RS** perovskite cannot possess a non-linear optical susceptibility of second order in the bulk of the material, we attributed the observed SHG effect to small impurities of the polycrystalline material that fall below the detection limit of the X-ray diffraction powder since the patterns are consistent with the calculated ones (Fig. S4, ESI†).

White-light emission

The photoluminescence of the three perovskites, **1R**, **1S** and **1RS**, was measured with an excitation wavelength of 315 nm. The centrosymmetric material **1RS** presents a sharper band (FWHM = 133 nm) than the other chiral perovskites **1S** (FWHM = 160 nm) and **1R** (FWMH = 164 nm), as shown in Fig. 3C. The chromaticity coordinates (CIE 1931) of the **1R** (0.30, 0.35) and **1S** (0.31, 0.37) are close to the ideal white light point (0.33, 0.33), while the emission of **1RS** (0.26, 0.32) can be described as cold white light with a maximum at 464 nm (Fig. 3D). Out of the three materials (**1R**, **1S** and **1RS**), **1RS** was found to be the brightest emitter, with a photoluminescence quantum efficiency (PLQE) of 6.1%, which is relatively high for white-light emitting perovskites (Table S1, ESI†).[9,21]

The photoluminescence of 2D HOIPs is highly sensitive to subtle structural distortion of the inorganic layer, which can be induced by the packing arrangement of the organic cation.[15] These materials (**1R**, **1S** and **1RS**) are clear examples of the latter, as subtle differences between the N–H···Br hydrogen bonds (see the X-ray diffraction data section in the ESI†), conformation of the β-MPA cation (see Fig. 2), and subsequent distortion of the inorganic layers of the perovskites are responsible for the differences in the PL spectrum (Fig. 3C). The effect of the cation can be addressed through the comparison of **1R**, **1S**, and **1RS**

Table 1 Average distortions for the Pb–Br bond lengths in **1RS**, **1R**, **1S** (this work), α-DMEN $PbBr_4$,[12] $EA_4Pb_3Br_{10}$,[13] and NMEDAPbBr_4.[35]

Perovskite	Average Δd_{Pb}
1RS	2.455×10^{-4}
1R	3.659×10^{-6}
1S	3.399×10^{-6}
α-DMEN $PbBr_4$ (DMEN = 2-(dimethyl amino)ethyl ammonium)[12]	17.4×10^{-4}
$EA_4Pb_3Br_{10}$ (EA = ethyl ammonium)[13]	40.74×10^{-4}
NMEDAPbBr_4 (NMEDA = 1*N*-methylethane-1,2-diammonium)[35]	3.854×10^{-4}

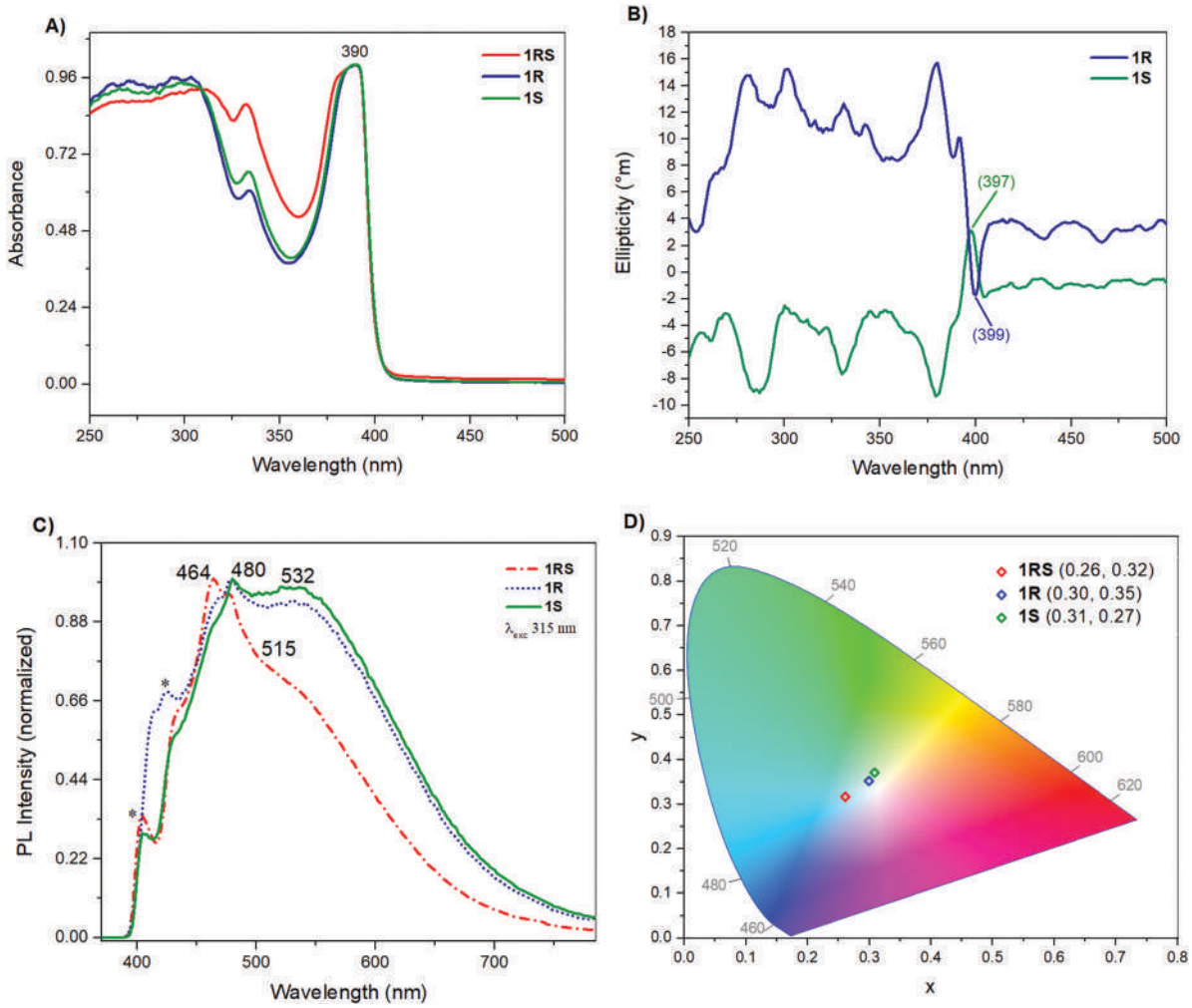

Fig. 3 (A) Absorbance spectra of **1R**, **1S** and **1RS**, (B) circular dichroism of **1R** and **1S,** (C) photoluminescence spectra of **1R**, **1S** and **1RS** and (D) CIE 1931 chromaticity coordinates of **1R**, **1S** and **1RS**.

with $(PEA)_2PbBr_4$ (PEA = 2-phenethylammonium) that exhibits a narrow purple emission,[40,41] with the difference being one methyl group that shortens the hydrogen bonds (N–H···Br) and distorts the inorganic layers (see the X-ray diffraction data section in the ESI†). Importantly, the fact that the **1S** and **1R** materials are both chiral and white light emitters suggests that they could also be of interest in circularly polarized white-light emission with applications in spin-LEDs.[42,43]

Conclusions

This work has shown how chiral organic cations can be used to tune the molecular geometry, chirality and, hence, the optical properties of HOIPs. For the first time, we show that the use of chiral organic cations led to non-centrosymmetric materials that emit white light and show SHG. The chromaticity coordinates of **1R** and **1S** are close to the ideal white point, whereas **1RS** emits cold white light. Although the second harmonic generation reported here is not exceptionally high, our results set a significant precedent and encourage others to rationally design 2D HOIPs with improved non-linear optical properties. Further research on the optical properties of this kind of materials is underway in our laboratories.

Conflicts of interest

There are no conflicts to declare.

Acknowledgements

We acknowledge the financial support from PAPIIT IA202418 and CONACYT's CB-A1-S-8729. We thank Dr Luis Ortiz-Frade, Dra. Maricela Cruz-Ramirez and CONACYT Infrastructure project (number 269102) for support and access to CD measurements. We also thank Adriana Tejeda, Carlos Ramos, Eriseth Morales, Alberto López, Alejandro Pompa, Cain González and Miguel Angel Canseco for their technical assistance. K. T. H. and G. R. L. thank CONACYT (grant 817844) and CONACYT-SENER (grant 488654) for their scholarships. P. S. H. and W. Z. thank the Welch Foundation (Grant E-1457) for support. G. P. was partly

supported through UNAM-PAPIIT IN107319 and INFR-2018-01-293349 from CONACyT.

Notes and references

1 A. K. Jena, A. Kulkarni and T. Miyasaka, *Chem. Rev.*, 2019, **119**, 3036–3103.
2 F. Zhang, D. H. Kim, H. Lu, J. S. Park, B. W. Larson, J. Hu, L. Gao, C. Xiao, O. G. Reid, X. Chen, Q. Zhao, P. F. Ndione, J. J. Berry, W. You, A. Walsh, M. C. Beard and K. Zhu, *J. Am. Chem. Soc.*, 2019, **141**, 5972–5979.
3 L. Gao, F. Zhang, X. Chen, C. Xiao, B. W. Larson, S. P. Dunfield, J. J. Berry and K. Zhu, *Angew. Chem.*, 2019, **131**, 11863–11867.
4 S. Adjokatse, H. H. Fang and M. A. Loi, *Mater. Today*, 2017, **20**, 413–424.
5 M. Bidikoudi, E. Fresta and R. D. Costa, *Chem. Commun.*, 2018, **54**, 8150–8169.
6 M. Worku, L. J. Xu, M. Chaaban, A. Ben-Akacha and B. Ma, *APL Mater.*, 2020, **8**, 010902.
7 S. Ye, F. Xiao, Y. X. Pan, Y. Y. Ma and Q. Y. Zhang, *Mater. Sci. Eng., R*, 2010, **71**, 1–34.
8 E. R. Dohner, A. Jaffe, L. R. Bradshaw and H. I. Karunadasa, *J. Am. Chem. Soc.*, 2014, **136**, 13154–13157.
9 M. D. Smith and H. I. Karunadasa, *Acc. Chem. Res.*, 2018, **51**, 619–627.
10 D. Cortecchia, J. Yin, A. Petrozza and C. Soci, *J. Mater. Chem. C*, 2019, **7**, 4956–4969.
11 D. B. Straus and C. R. Kagan, *J. Phys. Chem. Lett.*, 2018, **9**, 1434–1447.
12 L. Mao, Y. Wu, C. C. Stoumpos, M. R. Wasielewski and M. G. Kanatzidis, *J. Am. Chem. Soc.*, 2017, **139**, 5210–5215.
13 L. Mao, Y. Wu, C. C. Stoumpos, B. Traore, C. Katan, J. Even, M. R. Wasielewski and M. G. Kanatzidis, *J. Am. Chem. Soc.*, 2017, **139**, 11956–11963.
14 M. D. Smith, A. Jaffe, E. R. Dohner, A. M. Lindenberg and H. I. Karunadasa, *Chem. Sci.*, 2017, **8**, 4497–4504.
15 M. D. Smith, B. A. Connor and H. I. Karunadasa, *Chem. Rev.*, 2019, **119**, 3104–3139.
16 B. Febriansyah, D. Giovanni, S. Ramesh, T. M. Koh, Y. Li, T. C. Sum, N. Mathews and J. England, *J. Mater. Chem. C*, 2020, **8**, 889–893.
17 L. Mao, C. C. Stoumpos and M. G. Kanatzidis, *J. Am. Chem. Soc.*, 2019, **141**, 1171–1190.
18 J. Albero and H. García, *J. Mater. Chem. C*, 2017, **5**, 4098–4110.
19 Y. Dong, Y. Zhang, X. Li, Y. Feng, H. Zhang and J. Xu, *Small*, 2019, **15**, 1902237.
20 G. Long, R. Sabatini, M. I. Saidaminov, G. Lakhwani, A. Rasmita, X. Liu, E. H. Sargent and W. Gao, *Natl. Rev. Mater.*, 2020, **5**, 423–439.
21 F. Zhang, H. Lu, J. Tong, J. J. Berry, M. C. Beard and K. Zhu, *Energy Environ. Sci.*, 2020, **13**, 1154–1186.
22 M. Nespolo, M. Aroyo and B. Souvignier, *J. Appl. Crystallogr.*, 2018, **51**, 1481–1491.
23 C. Yuan, X. Li, S. Semin, Y. Feng, T. Rasing and J. Xu, *Nano Lett.*, 2018, **18**, 5411–5417.
24 J. Ma, C. Fang, C. Chen, L. Jin, J. Wang, S. Wang, J. Tang and D. Li, *ACS Nano*, 2019, **13**, 3659–3665.
25 P. Huang, K. Taniguchi and H. Miyasaka, *J. Am. Chem. Soc.*, 2019, **141**, 14520–14523.
26 Y. Peng, Y. Yao, L. Li, Z. Wu, S. Wang and J. Luo, *J. Mater. Chem. C*, 2018, **6**, 6033–6037.
27 K. M. Ok, E. O. Chi and P. S. Halasyamani, *Chem. Soc. Rev.*, 2006, **35**, 710–717.
28 *APEX 3, SAINT and SADABS*, Bruker AXS Inc., Madison, Wisconcin, USA, 2007.
29 *CrysAlisPro, Version 1.171.37.35, Agilent*, Now Rigaku Oxford Diffraction, Yarnton England, 2014.
30 *SCALE3 ABSPACK – An Oxford Diffraction program (C)*, 2005.
31 G. M. Sheldrick, *Acta Crystallogr., Sect. A: Found. Crystallogr.*, 2015, **71**, 3–8.
32 G. M. Sheldrick, *Acta Crystallogr., Sect. C: Struct., Chem.*, 2015, **71**, 3–8.
33 C. B. Hübschle, G. M. Sheldrick and B. Dittrich, *J. Appl. Crystallogr.*, 2011, **44**, 1281–1284.
34 O. V. Dolomanov, L. J. Bourhis, R. J. Gildea, J. A. K. Howard and H. Puschmann, *J. Appl. Crystallogr.*, 2009, **42**, 339–341.
35 E. R. Dohner, E. T. Hoke and H. I. Karunadasa, *J. Am. Chem. Soc.*, 2014, **136**, 1718–1721.
36 T. Ishihara, *J. Lumin.*, 1994, **60–61**, 269–274.
37 C. M. Mauck and W. A. Tisdale, *Trends Chem.*, 2019, **1**, 380–393.
38 A. Ben-Moshe, A. Teitelboim, D. Oron and G. Markovich, *Nano Lett.*, 2016, **16**, 7467–7473.
39 R. W. Boyd, in *Nonlinear Optics*, ed. W. R. Boyd, Elsevier, 3rd edn, 2008, pp. 69–133.
40 D. Liang, Y. Peng, Y. Fu, M. J. Shearer, J. Zhang, J. Zhai, Y. Zhang, R. J. Hamers, T. L. Andrew and S. Jin, *ACS Nano*, 2016, **10**, 6897–6904.
41 K. Shibuya, M. Koshimizu, F. Nishikido, H. Saito and S. Kishimoto, *Acta Crystallogr., Sect. E: Struct. Rep. Online*, 2009, **65**, m1323–m1324.
42 J. Wang, C. Zhang, H. Liu, R. McLaughlin, Y. Zhai, S. R. Vardeny, X. Liu, S. McGill, D. Semenov, H. Guo, R. Tsuchikawa, V. V. Deshpande, D. Sun and Z. V. Vardeny, *Nat. Commun.*, 2019, **10**, 1–6.
43 N. Nishizawa, K. Nishibayashi and H. Munekata, *Proc. Natl. Acad. Sci. U. S. A.*, 2017, **114**, 1783–1788.